

UC Irvine

UC Irvine Previously Published Works

Title

Experimental evaluation and comparative analysis of commercial variable-capacitance MEMS accelerometers

Permalink

<https://escholarship.org/uc/item/1ns934zv>

Journal

Journal of Micromechanics and Microengineering, 13(1)

ISSN

0960-1317

Authors

Acar, Cenk
Shkel, A M

Publication Date

2003

Peer reviewed

Experimental evaluation and comparative analysis of commercial variable-capacitance MEMS accelerometers

Cenk Acar and Andrei M Shkel

Department of Mechanical and Aerospace Engineering, Microsystems Laboratory, University of California at Irvine, Engineering Gateway 2110, Irvine, CA 92697, USA

E-mail: cacar@uci.edu and ashkel@uci.edu

Received 10 March 2003, in final form 30 April 2003

Published 28 May 2003

Online at stacks.iop.org/JMM/13/634

Abstract

This paper reports the experimental analysis of commercially available variable-capacitance MEMS accelerometers, characterized under standardized tests. Capacitive MEMS sensors of the same low-level input acceleration range with various mechanical sensing element designs, materials, fabrication technologies and price ranges were selected for evaluation. The selected sensors were characterized using ANSI and NIST certified testing equipment and under the same testing conditions; and their sensitivity, resolution, linearity, frequency response, transverse sensitivity, temperature response, noise level and long-term stability were tested and compared. The experimental results are then interpreted to provide an insight to advantages and disadvantages for using a particular mechanical design, fabrication technology, sensor material and the techniques for electronics integration and packaging of each specific sensor design.

(Some figures in this article are in colour only in the electronic version)

1. Introduction

With the continuously maturing micro-fabrication technologies, micromachined accelerometers have been successfully commercialized, and attained the second largest sales volume among MEMS devices after pressure sensors. Various MEMS accelerometers have been reported and commercialized employing a wide range of detection schemes, including piezoelectric, piezoresistive, capacitive, resonance, optical, magnetic, etc. In the inertial sensing market, capacitive micromachined accelerometers offer several benefits when compared to the piezoresistive or piezoelectric type accelerometers with their good DC response and noise performance, high sensitivity, low drift and low temperature sensitivity [1, 2].

While extremely rugged, piezoelectric accelerometers require a dynamic input of some minimum frequency to generate a response, and have limited low-frequency response capabilities. At low-frequency acceleration inputs, they

exhibit significant attenuation and phase shifts, limiting the applications [3]. For example, in motion measurement (i.e. inertial navigation, robot control or biomedical applications) the measured acceleration data must not contain any zero offset error, since the zero offset in the acceleration output leads to gross amount of velocity or displacement errors after numerical integrations.

Piezoresistive MEMS accelerometers are also attractive for most applications due to their low cost, easy implementation and simple detection electronics. Even though micromachined piezoresistive accelerometers are applicable in low-frequency or steady-state acceleration measurement, their operation temperature range is substantially limited. The thermal coefficient of resistivity of doped silicon is over two orders of magnitude larger than the thermal coefficient of capacitance attained by a capacitive accelerometer, in spite of the changes in capacitor geometry due to thermal expansion, rendering piezoresistive accelerometers significantly temperature sensitive compared to capacitive

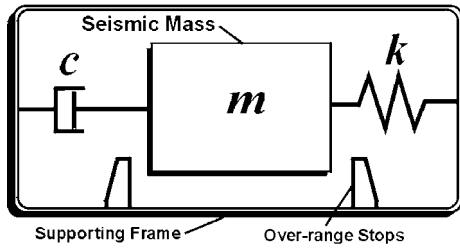


Figure 1. Dynamical mass-spring-damper model of an accelerometer.

accelerometers. More importantly, the frequency response of piezoresistive accelerometers is inherently temperature sensitive since the viscosity of the damping fluid used to eliminate resonant amplification and extend over-range capability is a strong function of temperature [4, 6]. Since the gaseous dielectric capacitors are relatively insensitive to temperature variations, capacitance sensing provides a wider temperature range of operation, without compensation, than piezoresistive sensing.

Various commercial capacitive MEMS accelerometers are available on the market, with similar performance specifications, but with completely different mechanical sensing element designs, materials, packaging and fabrication technologies and price ranges. However, very critical sensor parameters are not very well comparable from device to device using only the specifications provided by the manufacturer [3]. Some important parameters are not presented in specifications at all. To assess the suitability of a sensor for a specific application while maximizing the performance/cost ratio, side-by-side comparison of potential sensor designs is required. In this paper, we present the experimental results based on characterization and comparison of commercially available low- g capacitive MEMS accelerometers under standardized tests, using testing equipment certified by the American National Standards Institute and the National Institute of Standards and Technology. One off-the-shelf sample of each sensor was tested, which was certified by their manufacturer (no statistical analysis was performed in this work). The sensitivity, resolution, linearity, frequency response, transverse sensitivity, temperature effects, noise level and long-term stability of the selected sensors were tested; and the experimental comparison results were interpreted to assess the advantages and disadvantages of the mechanical design, fabrication technology, sensor material and the techniques of sensing electronics integration and packaging of each specific sensor design.

2. Capacitive MEMS accelerometers

Despite the variety of the employed detection schemes, every accelerometer can be modeled as a mass-spring-damper system (figure 1), where the proof mass deflects relative to its supporting frame with the input acceleration, forming a second-order system:

$$m\ddot{x} + c\dot{x} + kx = ma_{\text{input}}$$

where x is the displacement of the proof-mass m with respect to its frame, a_{input} is the external input acceleration, k is the

suspension stiffness and c is the damping coefficient. With the definition of the natural resonance frequency $\omega_n = \sqrt{k/m}$, and the quality factor $Q = \sqrt{km}/c$; the response can be expressed in the Laplace domain as

$$X(s) = \frac{mA(s)}{ms^2 + cs + k} = \frac{A(s)}{s^2 + \omega_n/Qs + \omega_n^2}.$$

For under-damped conditions, exciting the system at or near the resonance frequency results in very large amplitudes, while the response to excitations above ω_n is highly attenuated. At frequencies sufficiently lower than ω_n , the sensitivity of the accelerometer becomes independent of the excitation frequency. This ideal operation frequency band is defined as the *accelerometer passband*, usually ranging from $0.2\omega_n$ to $0.5\omega_n$ depending on the damping ratio [4].

Since the bandwidth of the passband is proportional to ω_n , there is a tradeoff between the dynamic range and the sensitivity ($S = x_{\text{static}}/a_{\text{input}} = m/k = 1/\omega_n^2$) of an accelerometer. To achieve an optimally flat passband, the damping of the system is generally designed to be critically damped, by setting the damping ratio $\zeta = c/2m\omega_n$ equal to $\sqrt{2}/2$ [13, 14].

In capacitive accelerometers, the deflection x of the seismic mass is detected by the change in capacitance of the parallel-plate formed by the mass and stationary electrodes. Generally, differential capacitive sensing scheme is employed in order to linearize the output, and to compensate drifts and interferences in the detection of the very small deflections (as small as in the order of Angstroms). By forming two variable capacitors on opposite sides of the seismic mass, a differential capacitive bridge is formed, where the deflection results in capacitance increase in one capacitor, and capacitance decrease in the other.

The damping of the dynamical system is predominantly determined by the viscous effects of the gas confined between the seismic mass and the stationary areas. The damping coefficient is adjusted by the pressure inside the device package, and the geometry of the seismic mass. Since the viscosity of air is not a strong function of temperature, capacitive accelerometers offer a more stable frequency response compared to devices utilizing viscous oil as a damper fluid [13]. To achieve high shock survivability, mechanical over-range stops are incorporated into the supporting frame to protect the suspension by preventing large deflections.

3. Characterized sensors

Four commercial capacitive MEMS accelerometers with low-level input acceleration range of $\pm 10g$ were selected for evaluation among large-volume manufacturers of accelerometers (tables 1 and 2). The main selection criterion was to compare devices with various mechanical sensing element designs, materials and fabrication technologies that are designed for the same input acceleration range. It should also be noted that the price of the selected sensors ranged from tens of dollars to several hundred dollars.

3.1. Endevco 7290A-10

The Endevco Model 7290A Microtron z -axis accelerometer line utilizes differential variable capacitance microsensors,

Table 1. Comparison of the properties of the evaluated sensors.

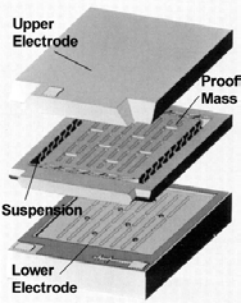
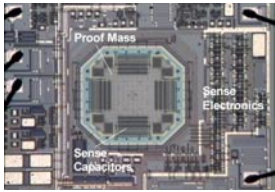
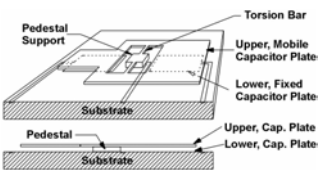
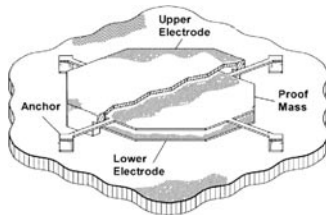
| Endevco 7290A-10 | Analog Devices ADXL210A | Silicon Designs SD2012-10 | Motorola M1220D |
|---|---|--|---|
|  <ul style="list-style-type: none"> • Out-of-plane • Bulk-micromachining • Two-chip • Single-crystal silicon |  <ul style="list-style-type: none"> • In-plane • Surface-micromachining • Integrated electronics • Polysilicon |  <ul style="list-style-type: none"> • Torsional • Electroforming • Two-chip • Nickel |  <ul style="list-style-type: none"> • Out-of-plane • Surface-micromachining • ‘Cap’ chip • Polysilicon |

Table 2. The capacitive MEMS accelerometers selected for evaluation, with the specifications supplied by the manufacturers.

| Manufacturer | Sensor | Range | Shock survivability | Sensitivity (mV/g) | Supply voltage (V _d) | Transverse sensitivity (%) | Temperature range (°C) |
|----------------|-----------|-------|---------------------|--------------------------|----------------------------------|----------------------------|------------------------|
| Endevco | 7290A-10 | 10g | 5000g | 200 mV/g | 15 | 2 | -55 +121 |
| Analog Devices | ADXL210A | 10g | 1000g | 20 mV/g × V _d | 5 | 2 | -40 +85 |
| Silicon Design | SD2012-10 | 10g | 2000g | 400 mV/g | 5 | 3 | -40 +85 |
| Motorola | M1220D | 8g | High | 50 mV/g × V _d | 5 | 5 | -40 +85 |

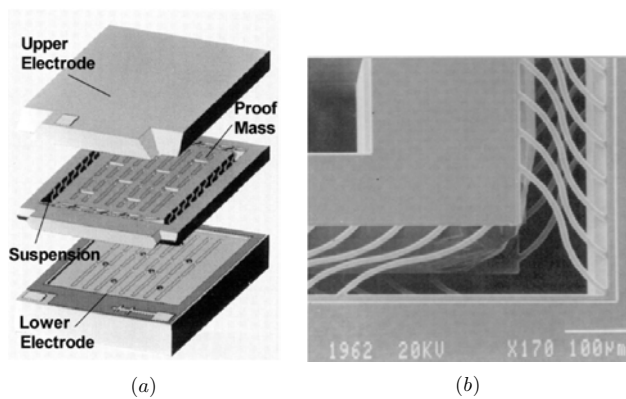


Figure 2. Endevco 7290A-10 accelerometer. (a) Structural design; (b) SEM micrograph of the suspension-beam array [13].

formed by bulk-micromachined thick proof mass that responds out-of-plane (figure 2). The device is made up of three single-crystal silicon wafers, joined together at the wafer level using an anodic bonding process. The top and bottom wafers contain the fixed capacitor plates, which are electrically isolated from the middle wafer by using thin layers of glass. The middle wafer contains the inertial mass, the suspension and the supporting frame. The suspension beam array is formed in the top and bottom surfaces of the middle wafer by diffusing boron dopant into both surfaces of the silicon wafer through the suspension pattern mask. The thickness of the beams is determined by the diffusion depth of the dopant, high concentrations of which render the fingers resistant to the etchant used to release the proof mass in the middle wafer. The proof-mass structure is then defined using

wet-etching techniques. After joining the three wafers, the devices are sliced into individual microsensors from the wafer array [13, 15].

Gas damping and internal over-range stops enable the anisotropically-etched silicon microsensors to withstand high shock and acceleration loads. Frequency response is controlled by the near-critically damped mass-spring system. The use of gas damping results in very small thermally-induced changes of frequency response. Electronics for the mechanical sensor is built on a separate ASIC chip, and wire bonded to the sensor chip.

3.2. Analog Devices ADXL210A

Analog Devices MEMS sensors are solid state accelerometers built using surface micromachining techniques. The ADXL210 is a complete, dual-axis acceleration measurement system on a single monolithic IC (figure 3), measuring acceleration along *x* and *y*-axes (in plane of the chip). It contains a polysilicon surface-micromachined sensor and signal conditioning circuitry to implement an open-loop capacitive acceleration measurement architecture.

The sensor is a surface micromachined polysilicon structure built on top of the silicon wafer, where polysilicon springs suspend the proof-mass structure over the surface of the substrate. Deflection of the structure is measured using a differential capacitor that consists of independent fixed electrodes and central electrodes attached to the moving mass. The fixed plates are applied 180° out of phase square waves. An input acceleration deflects the proof mass and unbalances the differential capacitor, resulting in an output square wave whose amplitude is proportional to acceleration. Phase sensitive demodulation techniques are then used to rectify the signal and determine the direction of the acceleration [8].

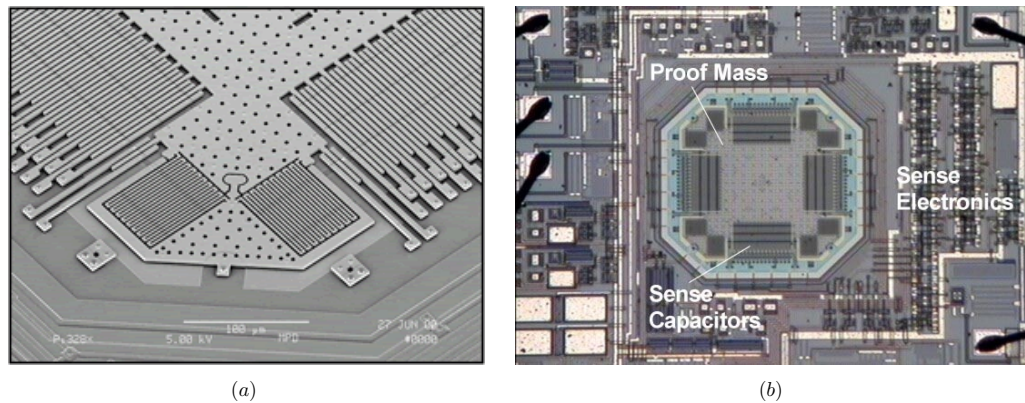


Figure 3. Analog Devices dual-axis accelerometer ADXL210A. (a) SEM micrograph of the suspension beams and the sensing capacitors; (b) micrograph of the integrated chip [8].

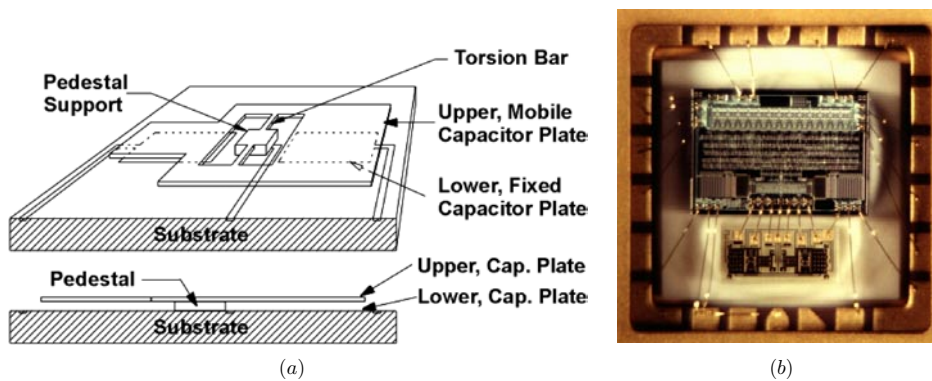


Figure 4. Silicon Designs SD2012-10 z -axis accelerometer. (a) Schematic illustration of the sensing element; (b) micrograph of the two-chip unit [9].

3.3. Silicon Designs SD2012-10

Silicon Designs SD2012-10 z -axis accelerometer is a two-chip unit consisting of the mechanical sensor chip and the integrated electronics chip. The chips are attached using standard die attach and gold wire bonding techniques, and the package is solder sealed to provide a fully hermetic device.

The sense element wing is a flat plate of nickel supported above the substrate surface by two torsional bars attached to a central pedestal. The asymmetric proof-mass structure has a center of mass that is offset from the axis of the torsional bars, so that an acceleration along the z -axis produces a moment around the torsional bar axis (figure 4). On the substrate surface, beneath the sense element wing, two conductive capacitor plates are symmetrically located on each side of the torsional bar axis. The upper wing and the two lower capacitor plates on the substrate form two air-gap variable capacitors with a common node, creating a fully active capacitance bridge. The sense element wings are approximately $1000\ \mu\text{m}$ long by $600\ \mu\text{m}$ wide and 5 to $10\ \mu\text{m}$ thick. The wing to substrate spacing of about 5 microns results in a capacitance from the wing to each lower plate of about $0.15\ \text{pF}$. Mechanical stops at the four outside corners of each sense element wing provide additional protection from overstress of the torsion bars under high shock conditions [9].

The sense element is built out of nickel and its alloys using selective electroforming, where the metal is electroplated onto a conductive substrate through a patterned photo-resist layer.

After the photo-resist has been stripped, the metal remains on the surface in a pattern determined by open areas of the photo resist. To produce suspended sense elements, the structure is fabricated partially on the top of a previously deposited sacrificial spacer material. After the sense elements have been formed, the spacer material is removed, leaving the sense element supported only where it was formed directly on the surface [9].

3.4. Motorola M1220D

Motorola M1220D is a two-chip z -axis MEMS accelerometer. The device consists of a surface micromachined capacitive sensing cell and a CMOS signal conditioning ASIC contained in a single integrated circuit package. The sensing element is sealed hermetically at the wafer level using a bulk micromachined 'cap' wafer. The mechanical structure is formed from polysilicon using masking and etching. It can be modeled as two stationary plates with a movable plate in-between (figure 5). The center plate can be deflected from its rest position by subjecting the system to an acceleration. When the center plate deflects, the distance from it to one fixed plate will increase by the same amount that the distance to the other plate decreases. The change in distance is a measure of acceleration. As the center plate moves with acceleration, the distance between the plates changes and each capacitor's value changes. The CMOS ASIC uses switched capacitor techniques to measure the capacitors and extract the acceleration data

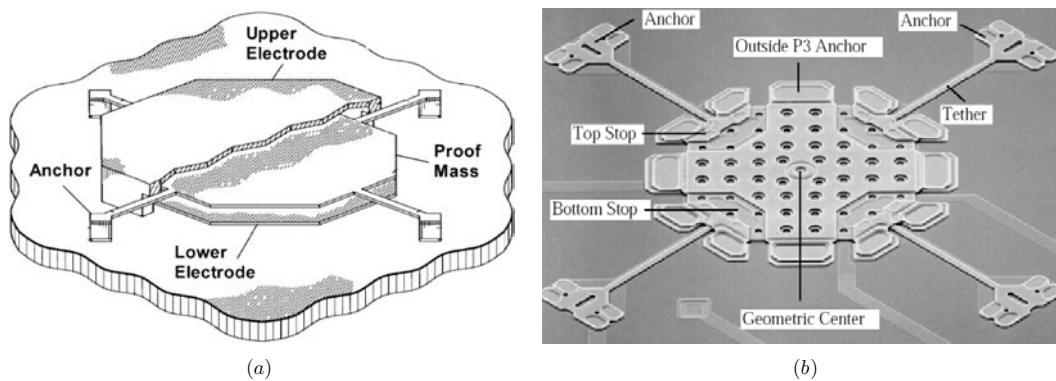


Figure 5. (a) Motorola MMA1220D z-axis accelerometer [10]; (b) micrograph of the sensing unit [11].

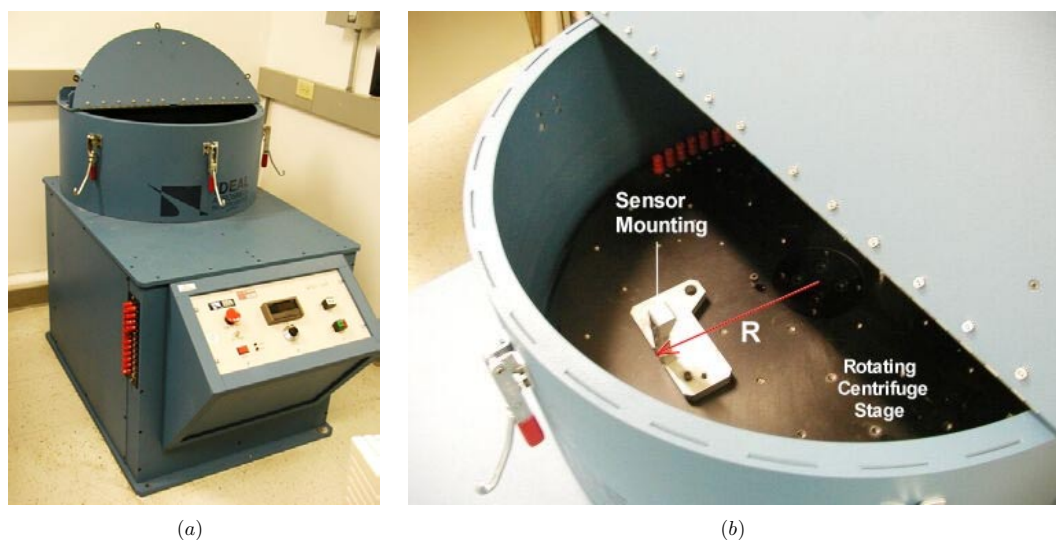


Figure 6. The Ideal Aeromsmith Inc Model 1068 centrifuge machine used in the linearity testing.

from the difference between the two capacitors. The ASIC also signal conditions and filters the signal, providing a high level output voltage that is ratiometric and proportional to acceleration [12].

4. Testing procedure

4.1. Sensitivity

The sensitivity of each device was first measured via a simple 2g turnover test, where the tested unit was subjected to +1g, 0g and -1g accelerations by rotating the sensitive axis in the 1g gravitational field. The sensitivity measurements were repeated using an Endevco Model 28952 automated accelerometer calibration system at various dynamic input frequencies. Finally, the sensitivity of the devices for DC inputs was verified using the computerized Klinger transverse sensitivity test machine, and Ideal Aeromsmith Inc centrifuge machine over the full input acceleration range.

4.2. Linearity

The linearity of the devices was measured using Ideal Aeromsmith Inc Model 1068 centrifuge machine [16]. The units were mounted on the horizontal centrifuge rotary table,

with their sensitive axes lying along the radius of the centrifuge (figure 6). The output of each unit was recorded for gradually increasing angular velocity, which is converted into the applied effective centrifugal acceleration, using the precise distance of the accelerometer center of mass from the centrifuge center. The same test was repeated for negative accelerations, by mounting the unit with the sensitive axis pointing the opposite direction. Maximum non-linearity and over-range of the devices were observed. The sensitivity of each device in positive and negative directions was also compared, which becomes critical in terms of bias shift due to vibration rectification (explained in section 5.2).

4.3. Frequency response

The frequency response of the sensors was measured using a computerized Endevco Model 28952 automated accelerometer calibration system. Two different shakers were used for low (1–200 Hz) and high (20–10,000 Hz) frequency band characterization (figures 7(a) and (b)). The amplitude and phase plots for each device in the low and high frequency bands were obtained. The frequency response tests reveal the sensitivity error and phase shift at the desired frequency, allowing to assess suitability of the sensor for various

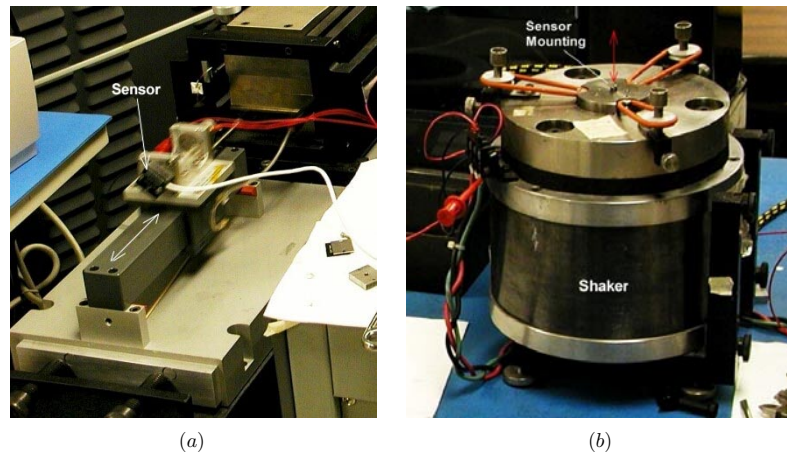


Figure 7. (a) Low-frequency shaker, and (b) high-frequency shaker of the Endevco Model 28952 automated accelerometer calibration system.

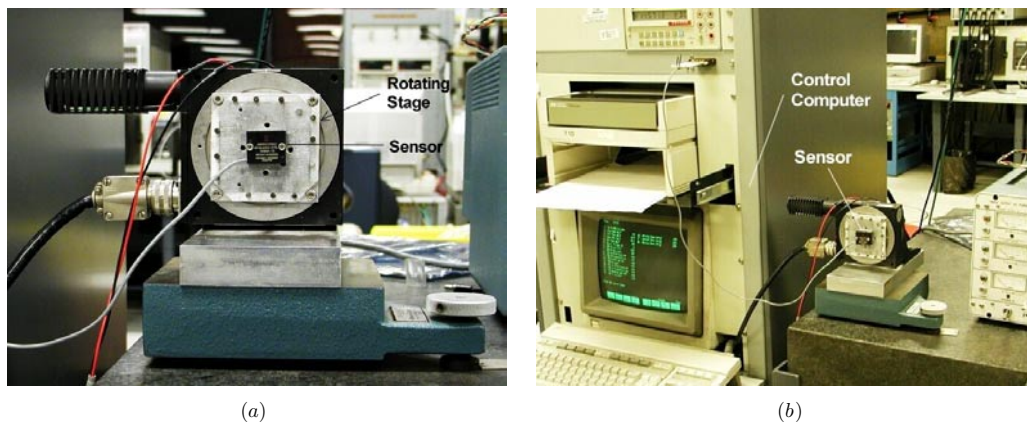


Figure 8. The Klinger transverse sensitivity test machine.

applications (civil, automotive, biomedical, etc) according to the dynamic response.

4.4. Transverse sensitivity

Maximum transverse sensitivity of the devices was measured using Klinger transverse sensitivity test machine (figure 8). The units were mounted on a horizontal shaft along their sensitive axes in a $1g$ field, and the shaft was rotated with computer control to determine the maximum sensitivity of the devices in the directions perpendicular to their sensitive axes.

4.5. Temperature response

The sensitivity of the sensors to temperature variations was characterized in an automated temperature-controlled chamber with computer-controlled $2g$ turnover stages (figure 9). The temperature of the chamber was stabilized and the units were soaked for 30 min at each programmed temperature from $-40\text{ }^{\circ}\text{C}$ to $+85\text{ }^{\circ}\text{C}$ before a $2g$ turnover test ($+1g$, $0g$, $-1g$ reading) was performed. The maximum sensitivity deviation, and maximum zero-measurand-output (ZMO)

deviation values in the full temperature range were calculated from the $2g$ turnover test results at each temperature step.

To measure the thermal hysteresis (ZMO hysteresis and sensitivity hysteresis) of each device, the zero shift and sensitivity shift were recorded for immediate temperature changes from $-40\text{ }^{\circ}\text{C}$ to $0\text{ }^{\circ}\text{C}$, and from $+85\text{ }^{\circ}\text{C}$ to $0\text{ }^{\circ}\text{C}$.

4.6. Noise level

The noise level of the units was measured using a Bruel&Kjoer Type 2425 Analog noise meter, which is basically an electronic voltmeter with a $1000\times$ amplifier (figure 10). The noise level of each unit was measured for different frequency bands (DC-100 Hz, DC-300 Hz and DC-1000 Hz). The tests were repeated after connecting the devices to a battery instead of a DC power source, in order to eliminate the added noise due AC-DC conversion in the power source.

4.7. Long-term stability

In order to determine zero-output stability, sensitivity stability and erratic behavior of the sensor over a long period time, $2g$ turnover tests ($+1g$, $0g$, $-1g$ output) for a period of 30 days were performed on each device. The zero-measurand-output

Table 3. Sensitivity testing results.

| Sensor | Specified sensitivity (mV/g) | Supply voltage (V _d) | Measured sensitivity (mV/g) | Measured sensitivity @ 100 Hz (mV/g) | Sensitivity error @ 100 Hz (%) |
|-----------|------------------------------|----------------------------------|-----------------------------|--------------------------------------|--------------------------------|
| 7290A-10 | 200 mV/g | 15.00 | 199.9 | 202.3 | +1.2 |
| ADXL210A | 20 mV/g × V _d | 5.00 | 108.0 | 107.7 | -0.3 |
| SD2012-10 | 200 mV/g | 5.00 | 399.3 | 401.3 | +0.5 |
| M1220D | 50 mV/g × V _d | 5.00 | 241.4 | 229.9 | -4.8 |

Table 4. Linearity testing results.

| Sensor | Specified over-range | Measured over-range | Positive sensitivity mV/g | Negative sensitivity mV/g | Positive-negative sensitivity difference (%) | Maximum non-linearity (%) |
|-----------|----------------------|---------------------|---------------------------|---------------------------|--|---------------------------|
| 7290A-10 | 10g | 19.4g | 198.6 | 198.2 | 0.20 | 0.251 |
| ADXL210A | 10g | 17.8g | 109.8 | 110.4 | 0.54 | 0.441 |
| SD2012-10 | 10g | 13.3g | 391.1 | 395.3 | 1.07 | 0.531 |
| M1220D | 8g | 10.8g | 248.8 | 252.3 | 1.39 | 0.694 |

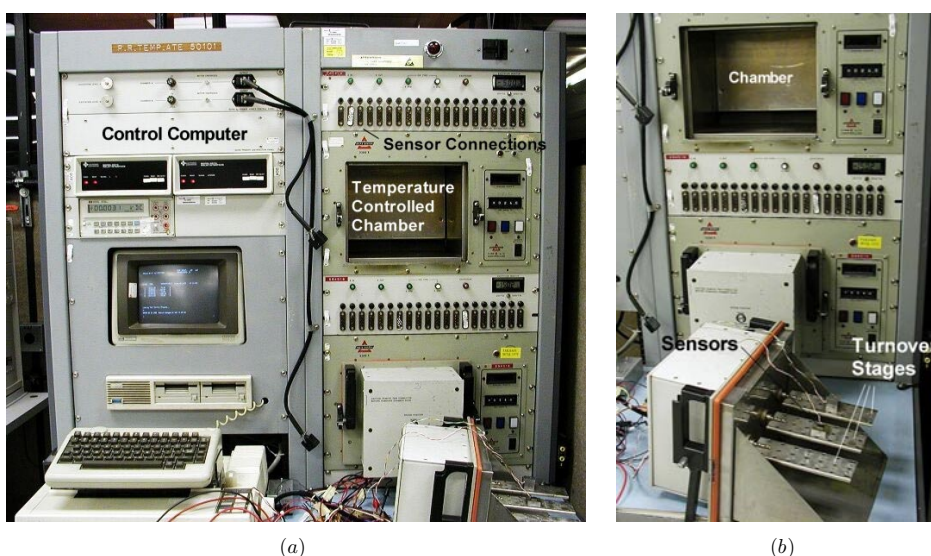


Figure 9. The automated temperature-controlled chamber with computer-controlled 2g turnover stages.

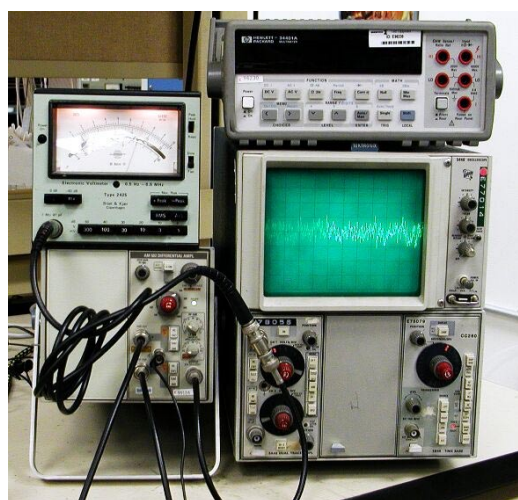


Figure 10. The Bruel&Kjoer Type 2425 Analog noise meter.

(ZMO) and sensitivity of each device were recorded to determine the maximum deviation in ZMO and sensitivity.

5. Experimental results

5.1. Sensitivity

The sensitivity test results obtained from the 2g turnover test and the Endeveco Model 28952 automated accelerometer calibration system for 100 Hz dynamic input are presented in table 3.

Endevco 7290A exhibited the least deviation of measured sensitivity from the specified sensitivity (0.05%), while analog devices ADXL210 exhibited the largest deviation (8%). At 100 Hz dynamic input, ADXL210 exhibited the least deviation in sensitivity from DC measurement (-0.3%), while Motorola M1220D exhibited the largest deviation (-4.8%).

5.2. Linearity

The maximum non-linearity, difference of positive and negative direction sensitivity and the over-range of the devices observed in the centrifuge test are tabulated in table 4.

The centrifuge test results indicated that the Endeveco 7290A displayed the most linear behavior in the specified input

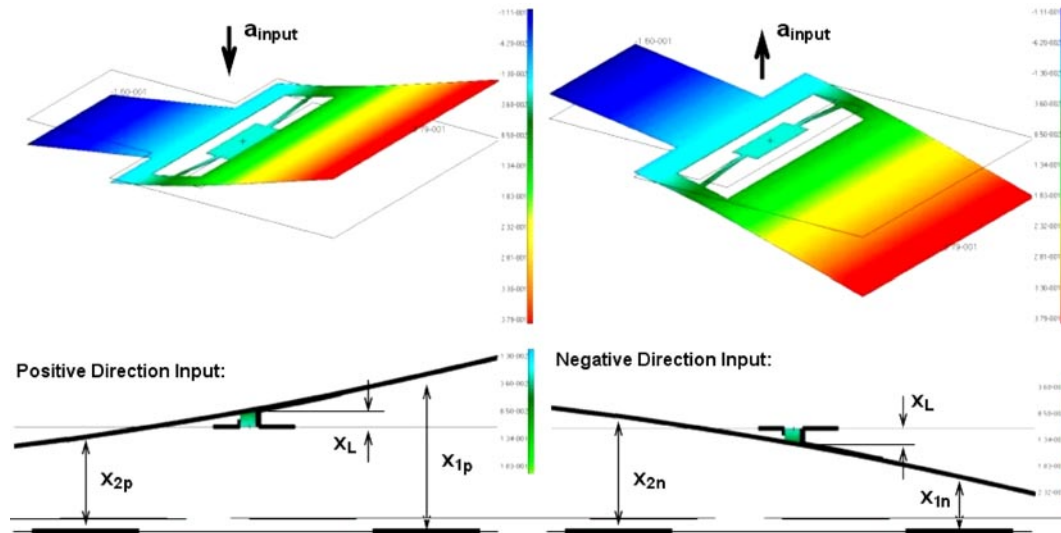


Figure 11. FEA simulations of a torsional accelerometer system with a structure similar to Silicon Designs SD2012.

range, with the least maximum non-linearity (0.25%FSO), and the least difference between the positive and negative direction sensitivities (0.20%). M1220D exhibited the largest non-linearity (0.69%FSO), and the largest sensitivity difference between the positive and negative directions (0.20%). The difference between the positive and negative direction sensitivities of a device potentially manifests itself in bias shift due to vibration rectification [13]. Under a purely sinusoidal acceleration input, even though the average of the input signal is zero, the output of the accelerometer is non-zero if the positive and negative direction sensitivities are not equal.

To illustrate the effect of asymmetry, the response of a torsional accelerometer system (similar in geometry to the non-symmetric structure of Silicon Designs SD2012) to positive and negative accelerations was simulated using the finite element analysis package MSC Nastran/Patran (figure 11). The FEA results indicated that the deflection due to the input acceleration is not purely torsional, and the undesirable out-of plane deflection of the structure (x_L) is also present. This forms the basis of sensitivity difference in positive and negative directions, and sensitivity shifts for different acceleration levels. Since the capacitive sensing electronics detect the difference of the capacitors in the differential bridge, undesirable linear deflections result in deviation in sensitivity. Referring to figure 11, the ratio of sensitivities in positive and negative directions for the same input magnitude is $S_n/S_p = (x_{1p}x_{2p})/(x_{1n}x_{2n})$. Assuming a $5 \mu\text{m}$ nominal gap and a $1g$ input, FEA results yield $x_{1n} = 4.69 \mu\text{m}$, $x_{2n} = 5.23 \mu\text{m}$, $x_{1p} = 5.31 \mu\text{m}$ and $x_{2p} = 4.77 \mu\text{m}$; leading to $S_n/S_p = 1.032$, which matches closely with the experimental difference of 1.07%.

The better symmetry of sensitivity in the forward and reverse axial directions of Endevco 7290A and ADXL210 can be attributed to their symmetry with respect to the axis of sensitivity. The fabrication process of Endevco 7290A, which involves bonding of three bulk-micromachined silicon layers at the wafer level, assures having the same gap between the upper and lower electrodes, and the moving plate.

Wafer-level bonding also minimizes the initial tilt angle of the moving plate with respect to the stationary electrodes, improving linearity.

In the case of ADXL210, which is fabricated using surface micromachining technology, the in-plane shuttle and the capacitor fingers are inherently axially symmetric due to the fabrication approach. All of the positive and negative direction air-gap capacitor fingers, and the moving mass fingers are formed out of the same sheet of polysilicon by lithography, and using the same fabrication mask. Thus, the gap between all of the fingers is determined by lithography and the etching process, providing excellent symmetry in the axial direction.

Endevco 7290A was observed to have the largest over-range capability, with the output saturating at 19.4g (194%FSO); even though the non-linear behavior was observed to increase in the over-range region. One interesting response observed in the Silicon Designs accelerometer was the snapping effect when the over-range was reached. The output voltage was observed to increase instantaneously from 4.69 V to 4.83 V at 13.2g, and the structure was released at 12.6g. This effect could be attributed to the stiction force at the area of contact between the seismic mass and the mechanical stops, and results in increased recovery time from an over-range shock. As an illustration, the contact area can be roughly estimated for an accelerometer structure with similar geometry. The total adhesion energy of the stiction surface is equal to the difference of elastic energy stored in the system just before snapping and just after releasing. It should be noted that the adhesion energy of the surface, assumed 50 mJ m^{-2} , is likely to vary over three orders of magnitude depending on surface termination and surface roughness [18]. When an example torsional system with comparable dimensions is considered (with a mass imbalance of $2.7 \times 10^{-8} \text{ kg}$, an effective stiffness of 0.03 N m^{-1} and a gap of $5 \mu\text{m}$) the area of contact is approximately estimated as $6.7 \mu\text{m}^2$. The stiction area estimation is reasonable for the device geometry and the fabrication technology, supporting the experimental results. Similar effects have not been observed in Endevco 7290-A, where the seismic mass displacement is reported as

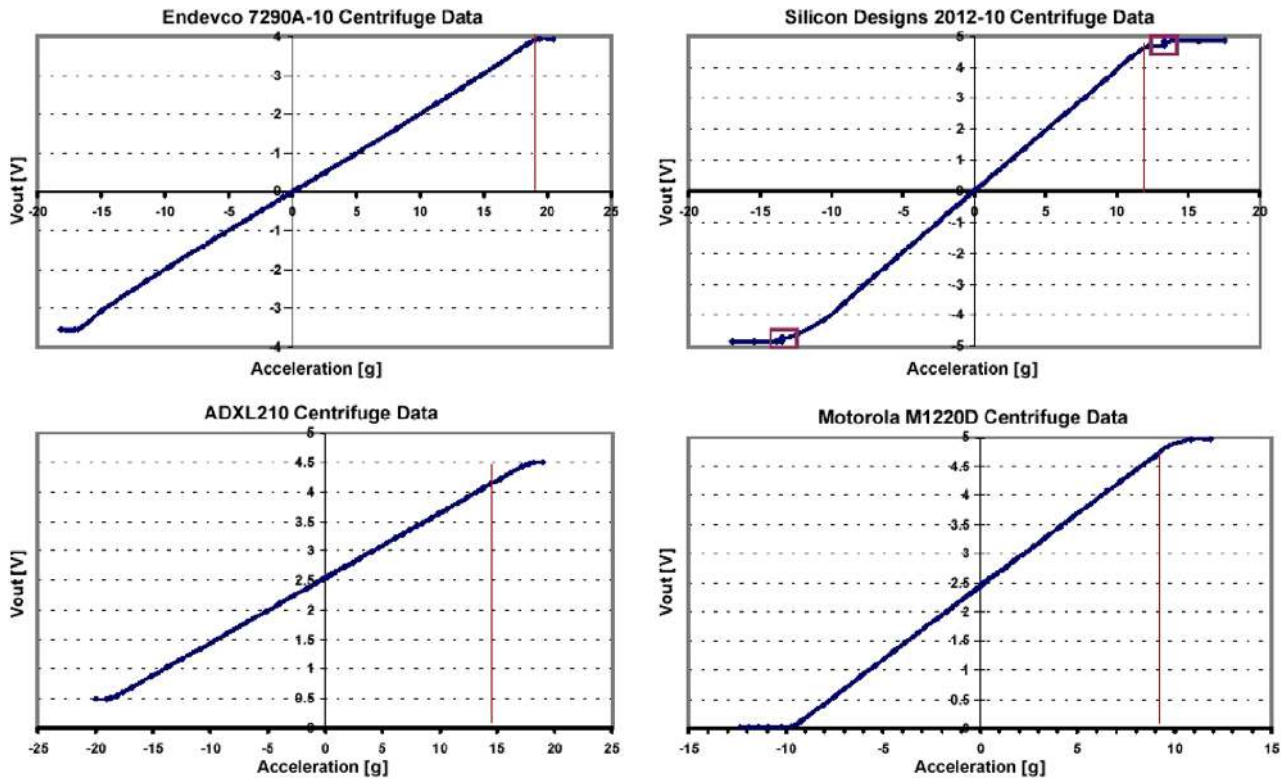


Figure 12. The centrifuge test results of the evaluated sensors.

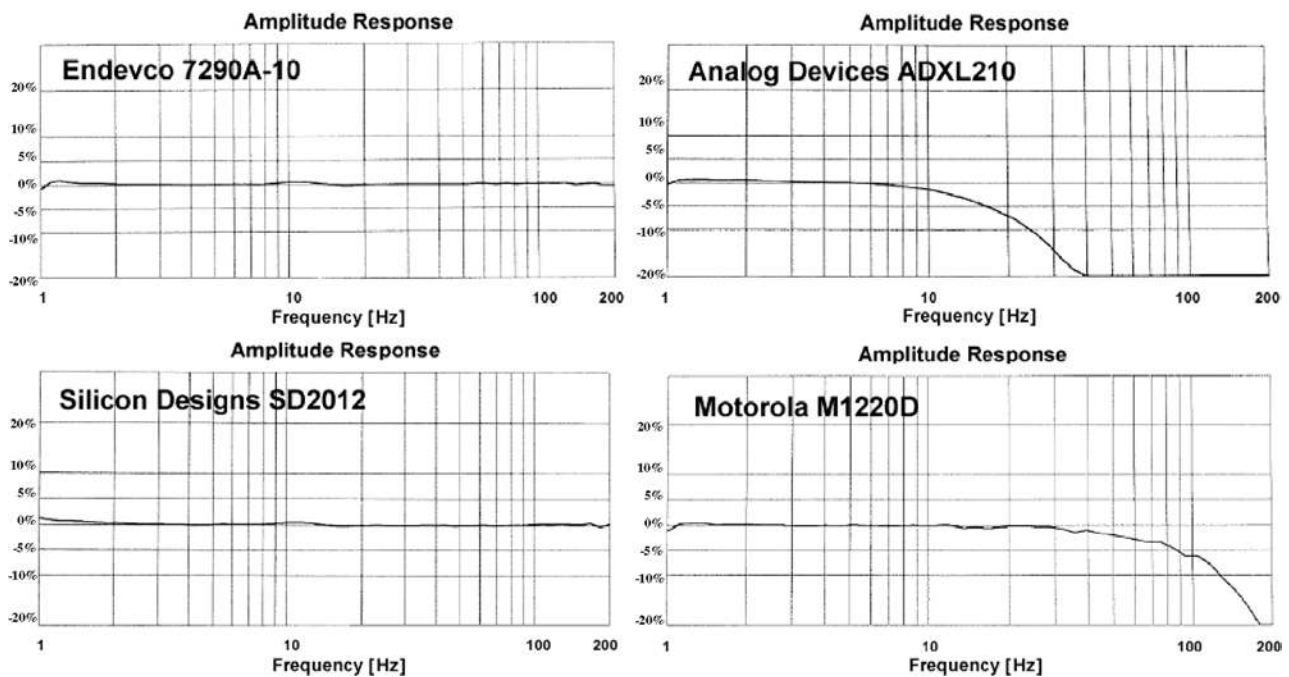


Figure 13. The frequency response amplitude plots of the evaluated sensors, in the 1–200 Hz range.

0.3 μm for full-scale, while the contact with the mechanical stops occurs at 0.6 μm displacement [15].

5.3. Frequency response

The low-frequency band (1–200 Hz) amplitude response of the sensors is presented in figure 13. From the frequency response

plots, it is observed that Endevco 7290-A and the Silicon Designs 2012 have remarkably flat frequency response in the 1–200 Hz frequency range. As seen in table 5, they provide the lowest amplitude and phase errors for dynamic inputs at 10 Hz, 100 Hz and 200 Hz.

The useful frequency range for each sensor is better reflected in table 6, where the dynamic input frequencies for

Table 5. Frequency response testing results, revealing the amplitude and phase errors at the given frequencies.

| Sensor | Error @ 10 Hz | | Error @ 100 Hz | | Error @ 200 Hz | |
|-----------|---------------|--------|----------------|-------|----------------|-------|
| | Amplitude (%) | Phase | Amplitude (%) | Phase | Amplitude (%) | Phase |
| 7290A-10 | 0.5 | +2° | 0 | -3° | -0.5 | -12° |
| ADXL210A | 3 | -12.2° | 40 | -50° | >100 | -55° |
| SD2012-10 | 1 | +2° | 0.5 | -3° | 0.5 | -15° |
| M1220D | 1 | -4.5° | 7 | -40° | 26 | -70° |

Table 6. Frequency response testing results, revealing the frequency range for the given amplitude and phase errors.

| Sensor | Amplitude error (Hz) | | Phase error (Hz) | |
|-----------|----------------------|------|------------------|------|
| | 5% | 10% | 45° | 90° |
| 7290A-10 | 1600 | 1900 | 1000 | 2030 |
| ADXL210A | 16 | 22 | 70 | 400 |
| SD2012-10 | 900 | 1200 | 700 | 1390 |
| M1220D | 90 | 120 | 90 | 180 |

Table 7. Transverse sensitivity testing results.

| Sensor | Specified transverse sensitivity (%) | Measured transverse sensitivity (%) |
|-----------|--------------------------------------|-------------------------------------|
| 7290A-10 | 2 | 0.863 |
| ADXL210A | 2 | 1.249 |
| SD2012-10 | 3 | 0.448 |
| M1220D | 5 | 2.742 |

5% and 10% amplitude errors, and 45° and 90° phase errors are tabulated. The frequencies where Endevco 7290A and Silicon Designs 2012 produce 5% sensitivity error are 1600 Hz and 900 Hz, respectively. The sensitivity error of ADXL210 reaches 5% at 16 Hz, while the sensitivity error of M1220D reaches 5% at 90 Hz. This makes 7290A and SD2012 much more suitable for DC-1kHz dynamic measurements. It should also be noted that the manufacturer's specifications report the bandwidth of ADXL210 to be expandable up to 5 kHz by trading-off resolution, with the adjustment of external circuit components [8].

5.4. Transverse sensitivity (cross-talk)

Maximum cross-talk of the devices measured using Klinger transverse sensitivity test machine is presented in table 7.

Silicon Designs accelerometer exhibited the least cross-talk (0.448%), while the Motorola sensor exhibited the largest cross-talk (2.742%). All of the sensors were well within the specified transverse sensitivity values.

The torsional mechanical structure of the Silicon Designs SD2012 provides reduced sensitivity to cross-axis accelerations. Since the device has two symmetrical electrodes placed underneath the moving structure, any cross-axis acceleration results in the same capacitance change in the two capacitors of the differential capacitive bridge.

In Endevco 7290A, the support-beam array positioned at the top and bottom surfaces of the moving mass wafer very effectively suppresses the transverse-axis motions of the mass. Planar symmetry and peripheral support structure of the seismic mass prevent it to displace along the sensitive axis in the presence of cross-axis accelerations.

5.5. Temperature response

The temperature response of the sensors measured in the computer controlled temperature chamber is presented in table 8. The maximum sensitivity deviation, maximum zero-measurand-output (ZMO) deviation, ZMO hysteresis and sensitivity hysteresis values were calculated from the 2g turnover test results at each temperature step.

The sensitivity of Silicon Designs SD2012 accelerometer was observed to deviate by over 5% from 25 °C to 85 °C. This result may be attributed to the temperature dependent Young's modulus of nickel, and thermally induced stresses in the suspension structure due to mismatch in thermal expansion between the nickel plate and the silicon substrate. For example, when the temperature is increased from 25 °C to 85 °C, the elastic modulus of nickel decreases from 204.41 GPa to 201.10 GPa, while the elastic modulus of silicon decreases from 163.01 GPa to 162.36 GPa [19]. The resulting change in the elastic modulus of nickel (1.62%) is over four times larger than that of silicon (0.39%). Since the sensitivity is inversely proportional to the elastic modulus of the structure, temperature variations result in larger sensitivity changes in the Silicon Designs device with nickel structure. Furthermore, the coefficient of thermal expansion of Nickel ($13.1 \times 10^{-6} \text{ }^\circ\text{C}^{-1}$) is over five times larger than silicon ($2.49 \times 10^{-6} \text{ }^\circ\text{C}^{-1}$), suggesting larger thermally induced stresses.

Even though M1220D did not exhibit significant deviation in sensitivity, its zero-measurand-output (ZMO) was observed to deviate the largest (0.76%) among other sensors. Also, largest hysteresis in sensitivity and largest hysteresis in ZMO was observed on Motorola M1220D, although it is specified to be temperature compensated.

5.6. Noise level

The noise test results indicated that Endevco 7290A, which has the largest sensing capacitance but off-chip sensing electronics, has the lowest noise level and the highest resolution (0.42 mg). Even though ADXL210 has integrated electronics together with the sensing element on the same chip, the signal-to-noise ratio of this device is smaller due to the relatively smaller sense capacitance area. Surface-micromachined Motorola M1220D exhibited the least signal-to-noise ratio, since off-chip sensing electronics is employed with small nominal sense capacitance (table 9).

5.7. Long-term stability

The maximum deviation in the zero-measurand-output and the sensitivity of the devices throughout four measurements of 2g

Table 8. Temperature response testing results.

| Sensor | Maximum sensitivity deviation (%) | Maximum ZMO deviation (%) | ZMO hysteresis -40 to 25 °C (%FSO) | ZMO hysteresis +85 to 25 °C (%FSO) | Sensitivity hysteresis (%) |
|-----------|-----------------------------------|---------------------------|------------------------------------|------------------------------------|----------------------------|
| 7290A-10 | 3.016 | 0.317 | -0.007 | 0.007 | 0 |
| ADXL210A | 0.926 | 0.111 | -0.089 | 0.089 | 0 |
| SD2012-10 | 5.038 | 0.655 | 0.035 | 0.029 | 0 |
| M1220D | 0.408 | 0.766 | -0.363 | -0.020 | 0.25 |

Table 9. Noise level testing results.

| Sensor | DC-100 Hz | DC-300 Hz | DC-1000 Hz | Sensitivity (mV/g) | DC-100 Hz resolution (mg) |
|-----------|-----------------|-----------------|-----------------|--------------------|---------------------------|
| 7290A-10 | 84 μ V rms | 110 μ V rms | 150 μ V rms | 199.9 | 0.42 |
| ADXL210A | 140 μ V rms | 150 μ V rms | 170 μ V rms | 108.0 | 1.29 |
| SD2012-10 | 250 μ V rms | 400 μ V rms | 700 μ V rms | 399.3 | 0.62 |
| M1220D | 1.2 mV rms | 1.7 mV rms | 1.9 mV rms | 241.4 | 4.95 |

Table 10. Long-term stability testing results.

| Sensor | Maximum ZMO deviation (%FSO) | Maximum sensitivity deviation (%) |
|-----------|------------------------------|-----------------------------------|
| 7290A-10 | 0.007 | 0.341 |
| ADXL210A | 0.111 | 0.000 |
| SD2012-10 | 0.138 | 0.125 |
| M1220D | 0.221 | 1.122 |

turnover test (+1g, 0g, -1g output) in 30 days are presented in table 10.

Endevco 7290A exhibited the highest zero stability with 0.007%FSO deviation in ZMO, while Motorola M1220D exhibited the lowest zero stability. The sensitivity of ADXL210 showed no deviation in the 30 day period, while the largest sensitivity deviation was observed in M1220D.

6. Conclusion

In this paper, the experimental characterization and comparison results of four commercially available variable-capacitance MEMS accelerometers (Endevco 7290A-10, Analog Devices ADXL210A, Silicon Designs SD2012-10 and Motorola MMA1220D) were reported. The sensitivity, resolution, linearity, frequency response, transverse sensitivity, temperature response, noise level and long-term stability of the selected sensors were tested using ANSI and NIST certified testing equipment.

In characterization, Endevco 7290A and ADXL210 displayed the most linear behavior in the specified input range, with the least maximum non-linearity, and the highest symmetry of sensitivity in the forward and reverse axial directions, thanks to their fabrication processes which provide geometrical symmetry with respect to the axis of sensitivity. The torsional structure of the Silicon Designs SD2012 with two symmetrical electrodes placed underneath the moving structure was observed to reduce sensitivity to cross-axis accelerations. In Endevco 7290A, the support-beam array positioned at the top and bottom surfaces of the moving mass wafer was also observed to suppress the transverse-axis motions of the mass very effectively. The use nickel

on silicon substrate in Silicon Designs SD2012 accelerometer was observed to result in deviation of sensitivity in the operation temperature range, mainly due to the temperature dependent Young's modulus of nickel, and thermally induced stresses in the suspension structure because of thermal expansion mismatch. Endevco 7290A, which has the largest sensing capacitance, exhibited the lowest noise level and the highest resolution, in spite of off-chip sensing electronics. Consequently, the reported results are expected to assist future MEMS accelerometer designs in terms of mechanical design, fabrication technology, sensor material selection and the techniques of sensing electronics integration.

Acknowledgments

This work is supported by the National Science Foundation Grant CMS-0223050, project manager Dr Shin-Chi Liu. The authors would also like to thank Endevco for providing access to their accelerometer characterization equipment.

References

- [1] Barbour N and Schmidt G 2001 Inertial sensor technology trends *IEEE Sensors J.* **1** 332-9
- [2] Yazdi N, Ayazi F and Najafi K 1998 Micromachined inertial sensors *Proc. IEEE* **86** 1640-58
- [3] Chu A Accelerometer selection based on applications *Endevco Technical Paper TP291*
- [4] Sill R D Minimizing measurement uncertainty in calibration and use of accelerometers *Endevco Technical Paper TP299*
- [5] Beliveau A, Spencer G T, Thomas K A and Roberson S L 1999 Evaluation of MEMS capacitive accelerometers *IEEE Des. Test Comput.* 1640-58
- [6] Olney D and Link B Shock and vibration measurement using variable capacitance *Endevco Technical Paper TP296*
- [7] Webpage <http://www.endevco.com>
- [8] Webpage <http://www.analogdevices.com>
- [9] Webpage <http://www.silicondesigns.com>
- [10] Semiconductor accelerometer having reduced sensor plate flexure *US Patent 5,814,727* Motorola, Inc
- [11] Li G and Tseng A A 2001 Low stress packaging of a micromachined accelerometer *IEEE Trans. Packaging Manuf.* **24** 18-25
- [12] Webpage <http://motorola.com/semiconductors/>

-
- [13] Sill R D A 70g full scale accelerometer designed to survive 100,000g overrange *Endevco Technical Paper TP300*
- [14] Fraden J 1996 *Handbook of Modern Sensors* (Berlin: Springer)
- [15] Whittier R and Connolly T Miniature accelerometers for measuring inertial motions and surviving high g shock inputs *Endevco Technical Paper TP303*
- [16] Webpage <http://www.ideal-aerosmith.com/1068-2.html>
- [17] Li G and Tseng A A 2000 Transient and impact dynamics of a micro-accelerometer *J. Mater. Process. Manuf. Sci.* **9** 143–56
- [18] Mastrangelo C H and Hsu C H 1993 Mechanical stability and adhesion of microstructures under capillary forces *J. Microelectromech. Syst.* **2** 33–55
- [19] JAHM Software, Inc. Material Properties Database v5.0 webpage <http://www.jahm.com>